COMPARISON OF EXPERIMENTAL RESULTS WITH THE NON-LINEAR VORTEX LATTICE METHOD CALCULATIONS FOR VARIOUS WING-CANARD CONFIGURATIONS

J. Rom*, B. Melamed** and D. Almosnino***
Technion - Israel Institute of Technology
Haifa 32000, Israel

Abstract

The experimental measurements of the aerodynamic characteristics of five close coupled wing-canard configurations up to moderately high angles of attack are compared with the calculated results by the improved version of the Non-Linear Vortex Lattice Method (NLVLM). Using this method, the aerodynamic coefficients, the rolled-up vortex trajectories and the pressure distributions are calculated. These calculations are performed for the five wing-canard configurations for which experimental data is available. These wing-canard models include various wing and canard geometries and the investigation covers the effects of varying canard deflections and canard positions relative to the wing. This investigation indicates that in addition to the increased maximum lift by delaying the vortex breakdown the canard enables added maneuverability by the variation of the lift to drag ratio (L/D) and the longitudinal stability coefficient (dC_m/dC_L) as a function of the angle of attack and canard deflection. The aerodynamic force characteristics which are evaluated by the NLVLM are found to be in reasonably good agreement with the experimental data up to vortex breakdown. Less favorable agreement is found in the comparisons of the moment coefficients and pressure distributions.

List of Symbols

AR	Aspect Ratio
b	wing span
c	wing chord
C_l	section lift coefficient based on wing chord
C_L	total lift coefficient based on wing planeform area
C_m	pitching moment coefficient
C_p	pressure coefficient, $\Delta p/q_\infty$
D	drag
l	body length
L	lift
M	Mach number
N	Total number of surface panels
p	pressure
q	dynamic pressure, $(1/2)\rho V^2$
S	wing planform area
x,y,z	cartesian coordinates
α	angle of attack

subscripts

c	chordwise
s	spanwise
∞	free stream conditions

Introduction

It is by now well established that improved aerodynamic performance of slender wing configurations at high angles of attack is achieved by the enhancement of the strength of the rolled-up vortices. At increasing angles of attack the induced lift due to these vortices (the non-linear contribution to the lift) is increasing as long as the strength of the rolled-up vortices continue to increase until these rolled-up vortices burst and the wing stalls. Therefore, strong aerodynamic effects can be achieved by utilizing means to enhance the strength of the vortices and delay vortex breakdown. The most commonly used methods are the generation of new strong vortices by various devices, such as: leading edge extensions (LEX, LEE), leading edge flaps, winglets, "saw tooth" extensions, strakes, vortex flaps, pylons and fences, slots and blowing of jets. All of these, in various combinations, generate vortices which are directed to interact with the main lifting rolled up vortices to induce the vortex strength augmentation.

The close coupled wing-canard configuration has the additional advantage of utilizing the movable canard as an aerodynamic control surface. In this case,the moveable canard generates, in addition to its lift and pitching moment, also strong vortices that augment the strength of the wing's rolled-up vortices which result in increased total lift at higher angles of attack due to the delay in the vortex breakdown. The flow field generated by these vortices will cause an upwash on the canard due to the wing and a downwash on the wing due to the canard that will affect the lift forces and the pitching moments on each one of these surfaces and therefore

*Lady Davis Professor, Dept. of Aerospace Engineering, Fellow AIAA
**Graduate Student, Dept. of Aerospace Engineering
***Research Fellow, Dept. of Aerospace Engineering

the total lift and the trim and control effectiveness of the wing-canard configuration. In the present investigation we will examine the capabilities of the NLVLM to evaluate the aerodynamic characteristics of the wing-canard configuration which is dominated by the interactions between the canard and the wing vortices.

It is generally assumed that the vortex flow over the slender wing with or without the canard can be predicted with relatively good accuracy by inviscid methods of analysis. It is clear that the generation process of the free vortices, which is started by the separation of the vortical shear layer from the body and/or the wing's surface (or at the sharp leading edges), is due to viscous effects. These viscous effects may be viewed as the result of the strong interaction between the viscous flow near the surfaces with the inviscid external flow. It is then assumed that once the shear layers separate from the surfaces or leave the sharp leading edges they roll up into the known "rolled-up leading edge vortices" and the resulting flow is from now on dominated by the inviscid vortical flow characteristics. This hypothesis is the justification for the various panel methods as well as the justification for the application of the recently developed Euler code methods (Refs. 1-4). The complexity, the difficulty and the high costs of the Euler code calculations for practical aerodynamic configurations at subsonic speeds is still rather formidable (Ref. 5). The subject of the present paper is to show that the evaluation of the aerodynamic characteristics of slender wing-canard configurations in subsonic flows at high angles of attack is much simpler and much more economical in calculation time and computer resources when the Non Linear Vortex Lattice Method (NLVLM), is used. The basic formulation of the NLVLM is presented in Refs. 6-10, and an improved version will be presented in this paper. Using this new version of the NLVLM, the calculated aerodynamic coefficients as well as the flow field structure are found to be in good agreement with experiments. Even the calculation of the pressure distributions is in reasonable agreement with the experimental data, sufficiently so, as to be accepted as a reasonable approximation for preliminary design purposes.

The classical linear Vortex Lattice Method (VLM) as presented in Ref. 6 is not capable to include the effects of the rolling-up of vortices in the computation scheme. The method of calculating the effects of the rolling-up of the free vortices was developed and is the basis of the NLVLM as presented in Refs. 7 and 8, for the calculations of the aerodynamic parameters of wings, including the close coupled wing-canard configurations. The application of the NLVLM to slender bodies of various cross sections is presented in Refs. 9-2. A review of the method and description of recent improvements in the calculation scheme are included in this paper.

Method of Calculation

The first step in the NLVLM calculation is to divide the surfaces of the configuration to small panels (quadrilateral or triangular) and to imbed in each one of these panels the appropriate potential singularities, which are the elementary solutions to the Laplace equation, such as horseshoe line vortices and source distributions. In the classical VLM the trailing vortices are kept in the plane of the lifting surfaces, therefore, all the aerodynamic coefficients vary linearly with angle of attack. In the NLVLM the trailing vortices are allowed to detach from the lifting surfaces into the free stream and follow the streamlines into the rolled-up vortex structure. For thick wings and for bodies the thickness effects are accounted for by the superposition of potential sources which are distributed on the panel surfaces. In the cases of wings with rounded leading edges and bodies of various shapes it is required to determine, independently, the shape and the position of the separation lines.

The strength of the vortices in each panel and the induced flow field are then calculated by solving the matrix equation using the procedures presented in Refs. 7-12. The trailing vortices are allowed to leave the lifting surfaces at all edges and on bodies along specified separation lines. The free vortices trajectories are calculated imposing a "cut-off" distance parameter to join vortices as they approach this limiting distance. The calculation procedure is presented in the flow chart of Fig. 1. The calculation process requires a double iterative procedure - an inner iteration and then the full iterative cycle. The program was modified so as to insure better criterion for convergence. The convergence is insured by checking the deviations of the values of the strength of all bound vortices in all panels (as was already presented in Refs. 11 and 12 for slender bodies) and also the convergence of the trajectories of all free vortices at every point of the calculated trajectories. These severe convergence criterions insure that after few iteration when these criterions are fulfilled the pressure distributions and the aerodynamic coefficients also are converged. The details of the modified program will be presented in a separate paper.

The Close Coupled Canard-Wing Configurations

Experimental data on five wing-canard configurations are available and published in Refs. 12-19. It is therefore possible to compare between the

results of the NLVLM calculations and these experimental data.

Two of these configurations are the European Test Models used for computer code verification - Models A and B, shown in Fig. 2a and 2b. Details of model A are given in Refs. 13 and 14 and the details of model B in Refs. 15 and 16. The other three models are the Technion models - the Cropped wing-canard, the Wide canard and the Narrow canard shown in Figs. 3a, 3b and 3c, respectively. Details of the Cropped wing-canard are given in Ref. 12 and those of the Wide and Narrow canards in Refs. 17, 18 and 19.

The European Model A has a 60° triangular wing and a 60° triangular canard -i.e. both wing and canard, AR=2.31. The canard span is 40% of the wing span. Both are attached to a flat fuselage, where the canard can be placed at various vertical and horizontal positions in relation to the wing and the canard can also be deflected as shown in Fig. 2a.

The European Model B, shown in Fig. 2b, has a cropped delta wing, 65° swept leading edge and AR=1.38. The canard has 60° sweep for the leading edge and 35° swept back trailing edge with AR=1.65, as seen in Fig. 2b, and the canard span is 44% of the wing span. The position of the canard is just forward of the wing as shown in the Fig. 2b.

The Technion Cropped Delta (CD) Model, shown in Fig. 3a, is the model investigated in Ref. 12. The wing planform is a moderate AR cropped delta having a triangular angle of 59° and AR=1.85, and a small trailing edge sweep angle of 4.1°. The canard planform is the same as that used in the Wide canard model, with AR=2.9, and an area which is 18% of the wing area. The position of the canard in relation to the wing is also shown in Fig. 3a.

The Technion Wide Canard (WC) Model, shown in Fig. 3b, has also a 60° triangular wing (AR=2.31) and a canard which is a cropped delta with a 60° swept leading edge and 35° swept back trailing edge (AR=2.9). The Technion Narrow Canard (NC) Model has a 60° triangular wing (AR=2.31) and a canard which is a 75° swept leading edge delta (AR=1), as shown in Fig. 3c. These models are similar to those used in the investigation presented in Ref. 17, except that in the present tests the wing has sharp leading edges and a flat upper surface. The canard can be placed at various vertical and horizontal positions and also can be deflected by the use of a series of spacers.

Results of the Calculations and the Experimental Measurements

The NLVLM program, the flow chart of which is presented in Fig. 1, enables the calculation of the vortex trajectories and the bound vortices strength (aerodynamic loads) in each panel of the wing and each panel of the canard. It is then possible to calculate the integrated aerodynamic forces and moments as well as the pressure distributions over the wing and the canard surfaces. It is also possible to draw the trajectories of the shed vortices and to observe graphically the rolling-up of the vortices and the variations in the positions of these vortices, which is an indication to the interaction between these vortex systems.

As a first test, the variation of the aerodynamic coefficients as a function of the angle of attack for the three main wing planforms: the 60° delta - wing of model A, the wing of model B and the cropped delta wing are presented in Figs. 4,5 and 6. The results of the experimental measurements are presented with the results of the NLVLM calculations of the aerodynamic coefficients, C_L, C_D and C_m as a function of the angle of attack α. The effect of the wide canard on the cropped delta wing is also indicated on Fig. 6.

The results for the wing-canard configurations European Models A and B with canard deflection angle $\delta_c = 0^{\circ}$, are presented in Figs. 7 and 8, respectively. The effects of the canard deflection angle δ_c for model A, including the comparison with the experimental results are shown in Fig. 9. The corresponding results for the Technion Models Wide Canard and Narrow Canard at various horizontal canard positions are shown in Figs. 10 and 11, respectively.

Since flow visualization techniques play an important role in providing insight to these intricate flow fields, it is interesting to compare the calculated trajectories of the free vortices shed from the canard and the wing with the experimental visualization results. Top view of the oil flow pattern on Model A is shown in Fig. 12a for $\alpha = 8.8^{\circ}$ and in Fig. 12b for $\alpha = 14.7^{\circ}$(from Ref. 13). The calculated vortex trajectories for these cases are superimposed on the visualization pictures in these figures. The vortex trajectories measured by schlieren photography on the Narrow Canard Model at $\alpha = 17^{\circ}$ are presented in Fig. 13a - top view and in Fig. 13b - side view (from Ref. 17). The calculated vortex trajectories are superimposed on these figures as well.

The variations of the lift to drag ratio as a function of the angle of attack, showing the effect of canard deflections, for the Wide and Narrow Canards Models are presented in Figs. 14 and 15, respectively.

The pressure distributions for the Wide Canard

and for Model B configurations with canard deflection angle $\delta_c = 0^\circ$, are shown in Fig. 16 and in Fig. 17, respectively. These figures include the measured pressure distributions presented in Refs. 13 and 20. The pressure distributions calculated by the NLVLM program are also shown.

Discussion

The calculated aerodynamic coefficients for the various delta wings alone (canard off configurations) indicate very good agreement with the experimental measurements as seen if Figs. 4, 5 and 6. The lift and induced drag coefficient are in very good agreement for the wings of Model B (Fig. 5) and the Cropped Delta model (Fig. 6) up to angles of attack of close to 30°, while for the wing of Model A the measured data is somewhat lower. This may be due to the effect of the presence of the fuselage which reduces the measured lift of the wing. There is also reasonable agreement with the measured and calculated pitching moments for both wings of Models A and B for angles of attack of up to 15° with increasing deviations as the angle of attack is further increased.

The lift and the induced drag coefficients for all five wing-canard configurations, presented in Figs. 6 to 11, indicate very good agreement between the measured data and the values calculated by the NLVLM program for angles of attack up to $\alpha = 25^\circ$. The agreement between the measurements and the NLVLM calculations includes also the effect of canard deflections, showing that this deflection has negligible effect on the lift and induced drag coefficients of the configurations, as seen in Fig. 9 for Model A and in Fig. 10 and 11 for the WC and NC models, respectively. The calculations of the pitching moments are in agreement with the experimental data only at low angles of attack, up to 10°, as seen in these figures. This large difference may be due to the inability of the present NLVLM program to simulate the correct vortex roll-up on the lifting surfaces, as is demonstrated in the visualization results (Figs. 12 and 13) and the pressure distributions (Figs. 16 and 17). It should be noted that the differences between the measured and calculated positions of the aerodynamic center, in percent of the mean aerodynamic chord, are for these cases in the range of 2% to 5%.

Both the experimental data and the NLVLM calculations indicate that the main effect of the canard deflection is in its effect on the variation of the pitching moment and therefore on the aerodynamic trim. A most interesting effect is observed in the variation of the lift to drag ratio, L/D, as a function of the canard deflection angle at various angles of attack, presented in Figs. 14 and 15 for the WC and NC models, respectively. This effect is extremely dramatic at low angles of attack, between 2° to 10° and is still has effects up to 15°, as seen in Figs. 14 and 15. These variations in the L/D values can be very useful for the aerodynamic performance of wing-canard configurations presented.

The oil flow visualization photographs taken for Model A at angles of attack of 8.8° (Fig. 12a) and 14.7° (Fig. 12b) are used to examine the calculated vortex trajectories by the NLVLM program. It can be seen that at the low angle of attack, $\alpha = 8.8^\circ$, the vortex trajectories both on the canard and on the wing follow reasonably well the oil flow pattern. In this case we can expect also reasonable agreement between the measured and calculated pitching moment coefficient, as seen in Fig. 7. At $\alpha = 14.7^\circ$ it is seen that the calculated vortex trajectories indicate that the rolling-up of the vortices on the canard and on the wing is much slower than the actually measured pattern of the oil flow, as seen in Fig. 12b. This means that in the NLVLM calculations the pressures on the forward part of the wing are high in comparison with the experimental data and therefore the measured and calculated pitching moments are different, as seen in Fig. 7. Similar patterns are seen also on the Narrow Canard model using shlieren visualization, presented in Figs. 13a - top view and 13b - side view.

The comparison between the measured and the calculated pressure distributions on the Wide Canard and on Model B configurations at moderate angles of attack are shown in Figs 16 and 17, respectively. It is clear that the present NLVLM program does not simulate the correct vortex pattern on the wing and therefore the computed pressure distributions are distorted in comparison to the experimental measurements.

Summary and Conclusions

The present study of various wing planforms and wing-canard configurations and the comparison between the aerodynamic characteristics evaluated by the NLVLM program and the experimental measurements can be used to examine the merit of the NLVLM as a working program for aerodynamic design. The calculations of a complete wing-canard configuration requires about 10 to 20 minutes on an IBM 3081 class computer. This enables a relatively fast turn around computing time in design calculations. This time can be compared to reported Euler Code calculations requiring hours of Cray class computers. It is seen that the NLVLM program is capable to calculate within engineering accuracy the lift and induced drag coefficients of wing-canard configurations. Although the fuselage was not included in the present studies, it is possible to simulate a complete aircraft

configuration by the NLVLM program. The calculations of the pitching moment variations and the pressure distributions are less accurate and further studies are required to accelerate the rolling-up of the vortices over the lifting surfaces.

References

1. Rizzi, A., Eriksson, L.E., Schmidt, W. and Hitzel, S.M., "Simulating Vortex Flows Around Wings", AGARD CP No. 342, April 1983, pp 21.1-21.14

2. Murman, E.M. and Rizzi, A., "Application of Euler Equations to Sharp Edge Delta Wings with Leading Edge Vortices", AGARD Symposium on Application of Computational Fluid Dynamics in Aeronautics, Aix-en-Provence, France, April 1986.

3. Scherr, S. and Das, A., "Basic Analysis of the Flow Fields of Slender Delta Wings Using the Euler Equations", ICAS Paper 88-5.9.2. Proceedings of the 16th ICAS Congress, Jerusalem Israel, August 1988. pp 1428-1436.

4. Lee, K.D. and Brandt, S.A., "Modeling of Vortex Dominated Flow fields in the Euler Formulation", ICAS Paper 88-5.9.3. Proceedings of the 16th ICAS Congress, Jerusalem Israel, August 1988, pp 1437-1450.

5. Kandil, O.A. and Chuang, A.H., "Influence of Numerical Dissipation on Computational Euler Equations for Vortex Dominated Flows" AIAA Journal, Vol. 25, No.11, 1987, pp 1426-1434.

6. Margason, R.J. and Lamar, J. E., "Vortex Lattice Fortran Program for Estimating Subsonic Aerodynamic Characteristics of Complex Planforms", NASA TN D-4739, August 1968.

7. Gordon, R. and Rom, J., "Calculation of Aerodynamic Characteristics of Wings with Thickness and Camber by a New Method Based on the Modified Vortex Lattice Method", Technion-Israel Institute of Technology, TAE No. 493, July 1982.

8. Gordon, R. and Rom, J., "Calculation of Non-Linear Subsonic Characteristics of Wings with Thickness and Camber at High Incidence", AIAA Journal, Vol. 23, No. 6, June 1985, pp 817-825.

9. Almosnino, D. and Rom, J., "Calculation of Symmetric Vortex Separation Affecting Subsonic Bodies at High Incidence", AIAA Journal, Vol. 21, No. 3, 1983, pp 398-406.

10. Almosnino, D., "High Angle of Attack Calculations of the Subsonic Flow on Slender Bodies", AIAA Journal, Vol. 23, No. 8, 1985, pp 1150-1156.

11. Almosnino, D. and Rom, J., "Subsonic Aerodynamic Prediction of Shuttle - Like Configurations Using Non-Linear Vortex Lattice Method", ICAS Paper 88-4.4.2. Proceedings of the 16th Congress of ICAS, Jerusalem Israel, August 1988, pp. 638-643.

12. Rom, J., Almosnino, D. and Gordon, R., "High Angle of Attack Subsonic Non-Linear Vortex Flow Calculations", AIAA Paper No. 87-2275, August 1987.

13. Hummel, D. and Oelker, H.C., "Vortex Interference Effects on Close-Coupled Canard Configurations in Incompressible Flow", Proceedings of the International Vortex Flow Experiments on Euler Code Validation", Held in Stockholm Sweden, Oct. 1986. pp 47-61.

14. Oelker, H.C. and Hummel, D., "Investigation on the Vorticity Sheets of a Close-Coupled Delta Canard configuration", ICAS Paper 88-5.4.1. Proceedings of the ICAS Congress, Jerusalem Israel, August 1988, pp 649-662.

15. Drougge, G., "The International Vortex Flow Experiment for Computer Code Validation", ICAS Von-Karman Lecture, Paper 88-0.5, Proceedings of the ICAS Congress, Jerusalem, Israel, August 1988.

16. Hummel, D., Private Communications, Sept. 1988.

17. Er-El, J. and Seginer, A., "The Leading Edge Vortex Trajectories and Breakdown Characteristics of Close-Coupled Wing-Canard Configurations", Journal of Aircraft, Vol. 22, August 1985, pp 641-648.

18. Rom, J. and Er-El, J., Aerodynamic Characteristics of Close Coupled Canard Configurations Measured in the Subsonic Wind-Tunnel", T.A.E. Rept. 637, 1990.

19. Rom, J., Er-El, J. and Gordon, R., "Measurements of the Aerodynamic Characteristics of Various Wing-Canard Configurations and Comparison with NLVLM Results", AIAA Paper 89-2217, August 1989.

20. Er-El, J., "Effect of Wing/Canard Interference on the Loading of a Delta Wing", Journal of Aircraft, Vol 25, January 1988, pp 18-24.

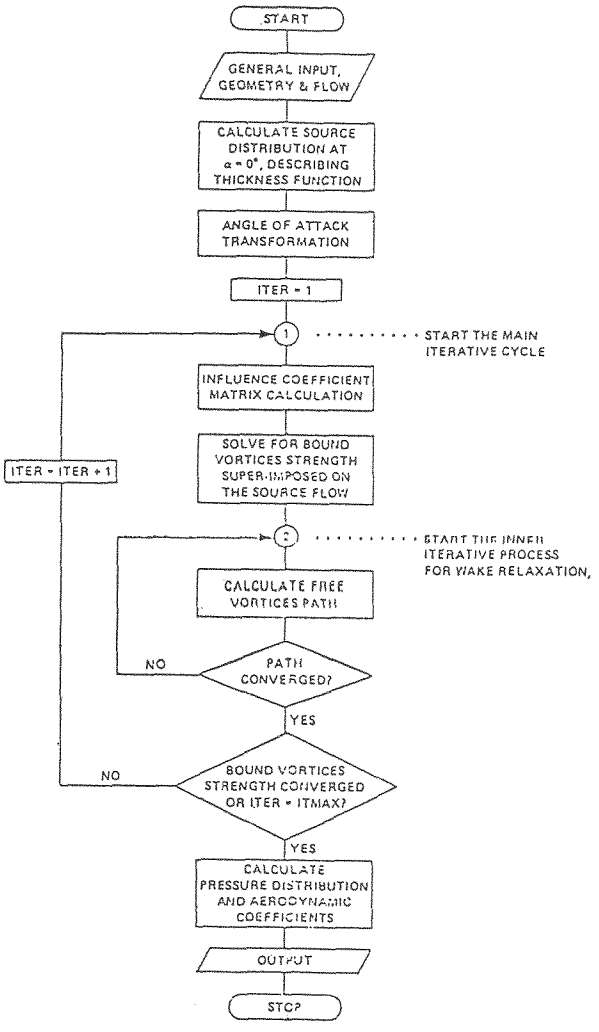

Fig. 1. Flow Chart for the NLVLM

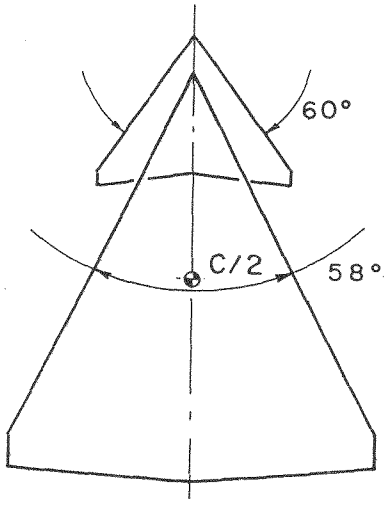

Fig. 3a. The Cropped Delta Wing-Canard Model

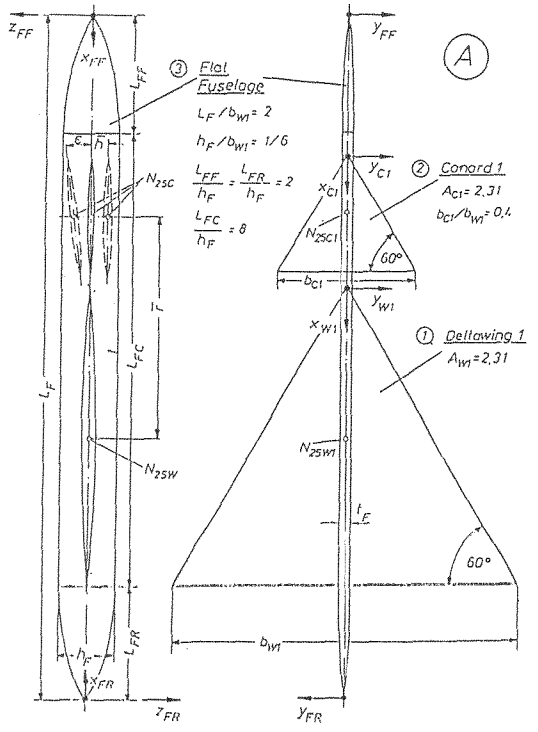

Fig. 2a. The Wing-Canard European Model A

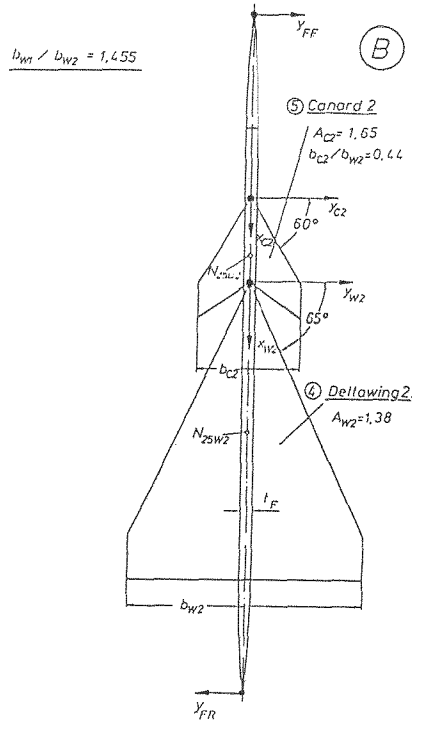

Fig. 2b. The Wing-Canard European Model B

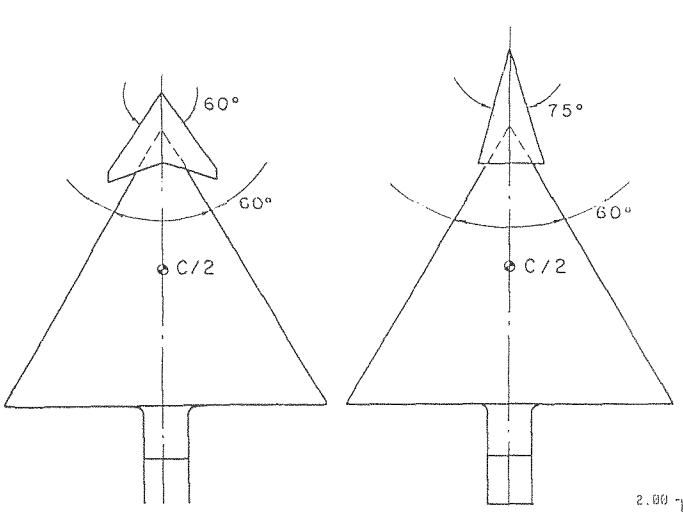

Fig. 3b. The Wide Canard Wing-Canard Model

Fig. 3c. The Narrow Canard Wing-Canard Model

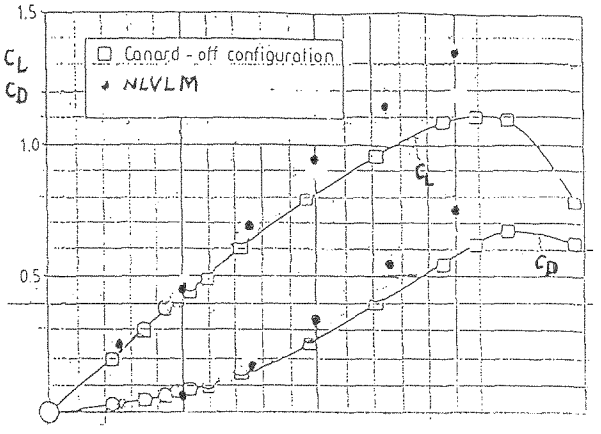

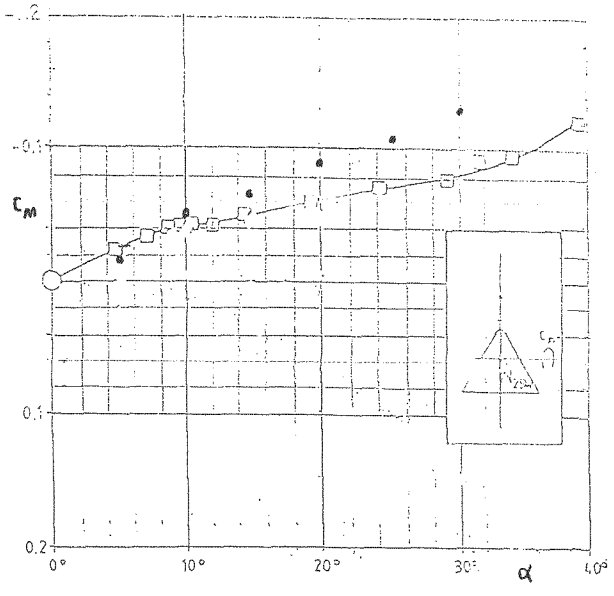

Fig. 4. The Variation of the Aerodynamic Coefficients of the 60° Delta Wing (wing of Models A and WC) as a function of α

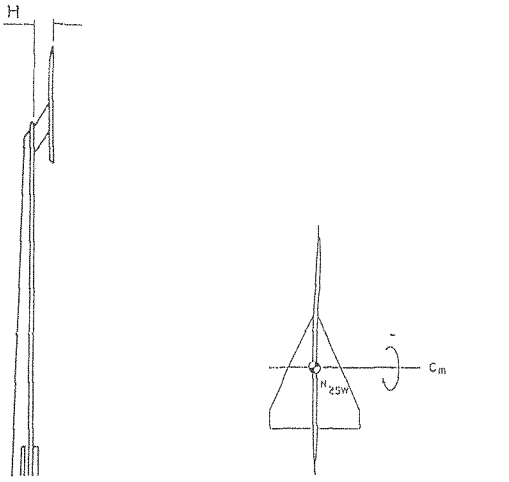

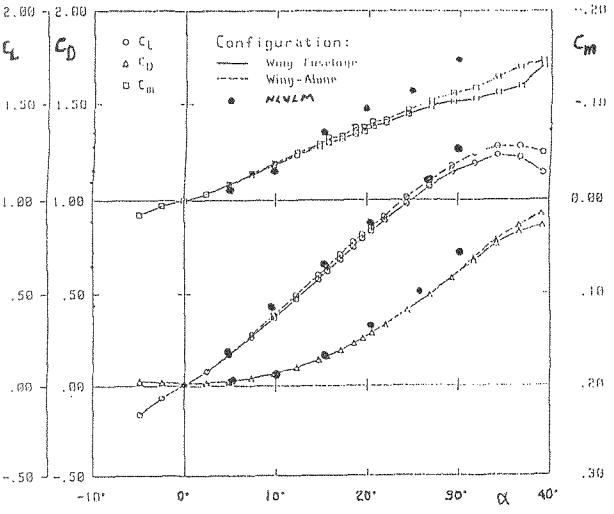

Fig. 5. The Variation of the Aerodynamic Coefficients of the Wing of Model B as a function of α

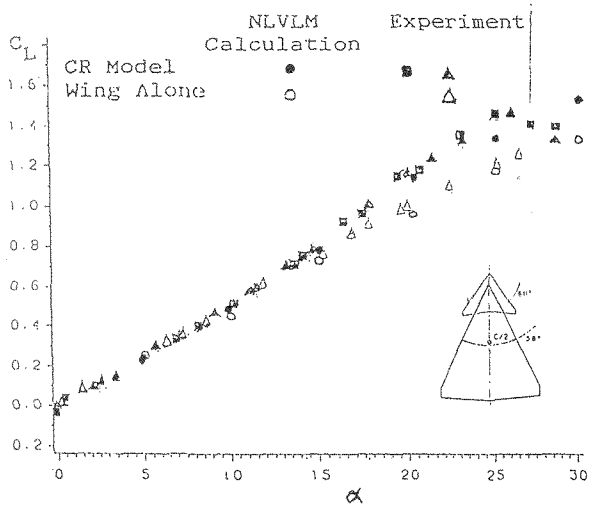

Fig. 6. The Variation of the Lift Coefficient as a function of α for the Cropped Delta Wing Alone and the Wing-Canard at x/c = 0.1

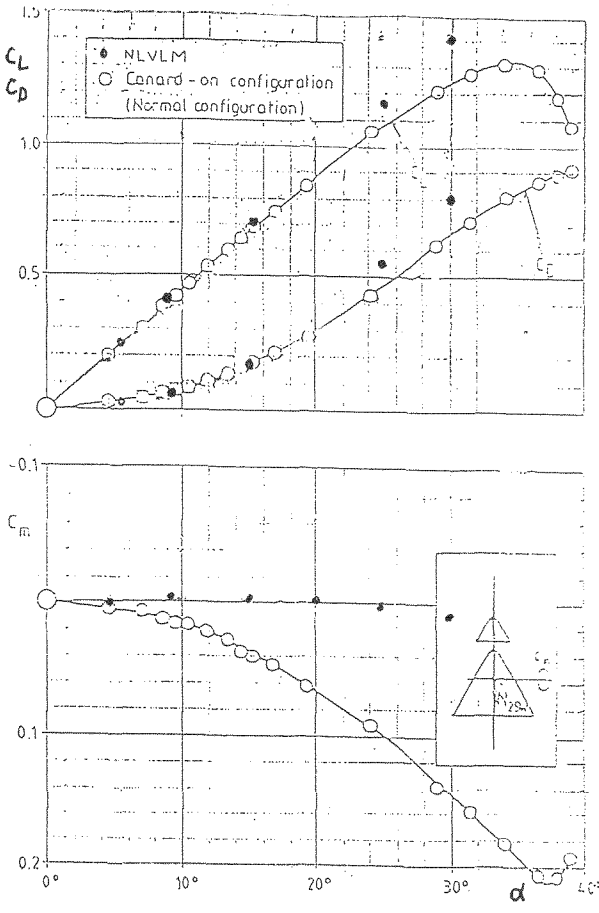

Fig. 7. The Variation of the Aerodynamic Coefficients as a function of α for the Wing-Canard European Model A at $\delta_c = 0$

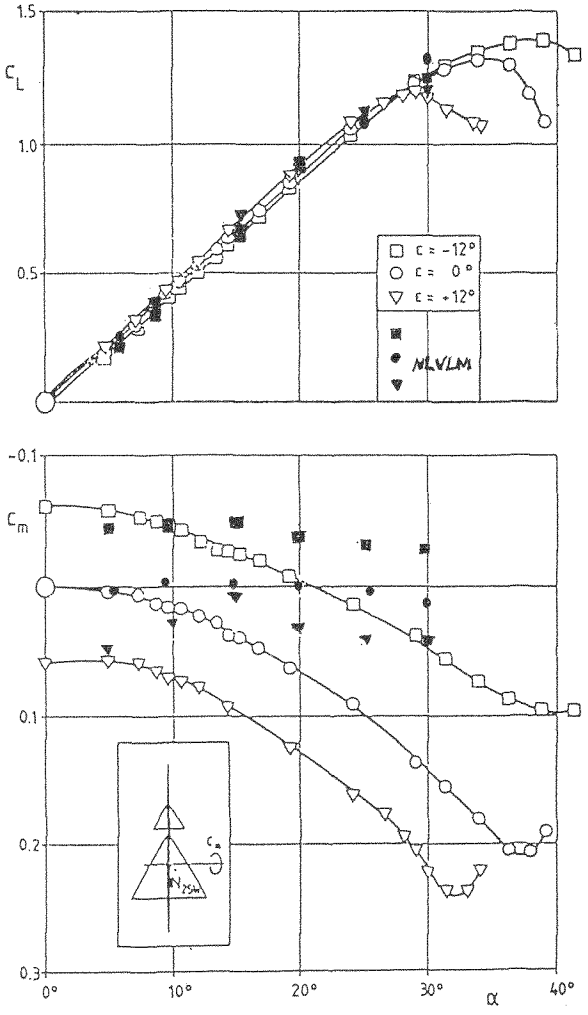

Fig. 9. The Effect of Canard Deflection on the Aerodynamic Coefficients of the Wing-Canard European Model A

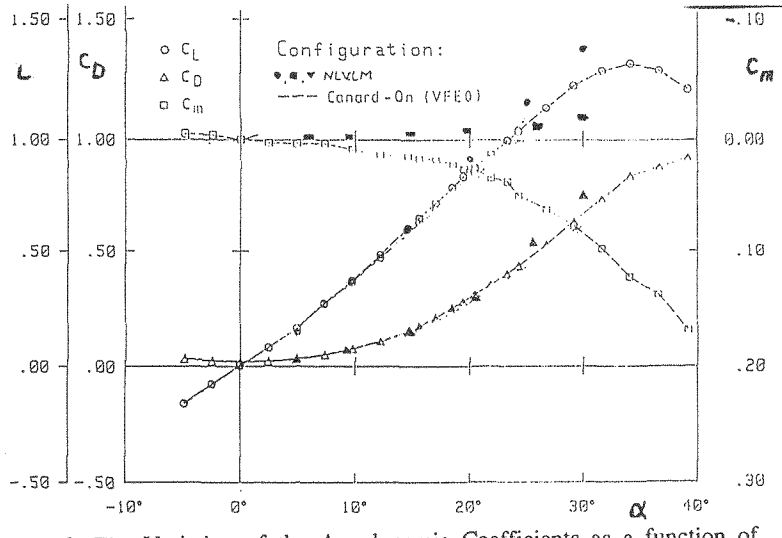

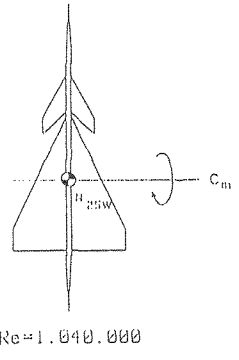

Fig. 8. The Variation of the Aerodynamic Coefficients as a function of α for the Wing-Canard European Model B at $\delta_c = 0$

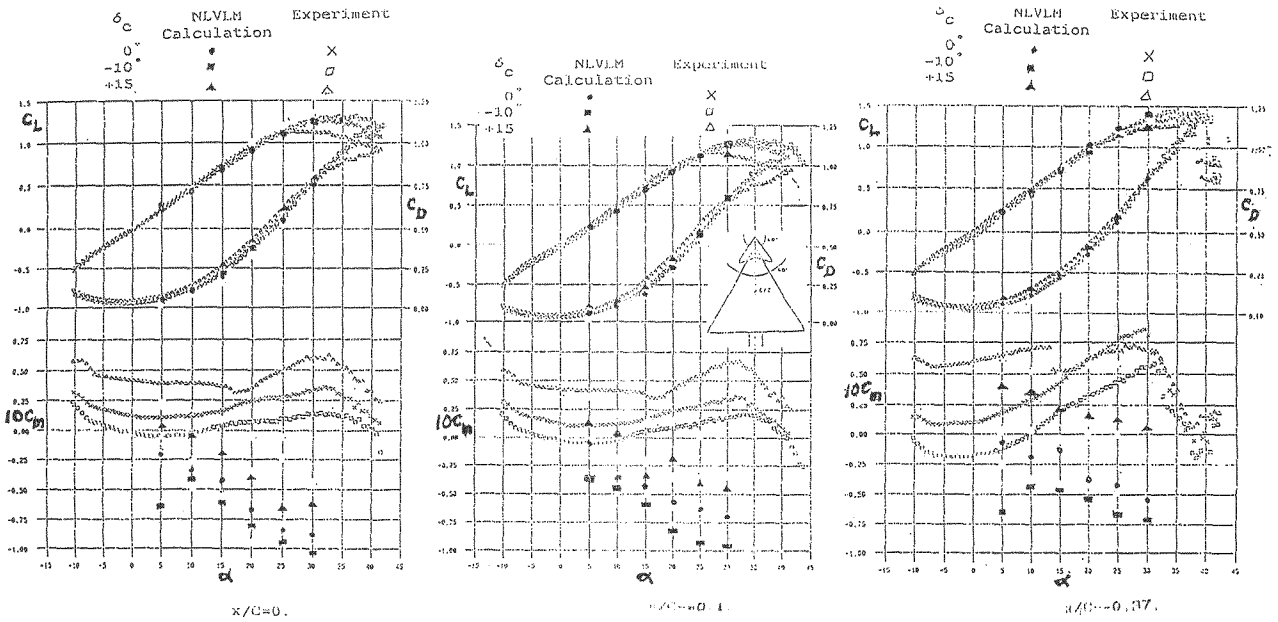

Fig. 10. The Variation of the Aerodynamic Coefficients as a function of α for the Technion Wide Canard Model at δ_c= -10°, 0°, +15°

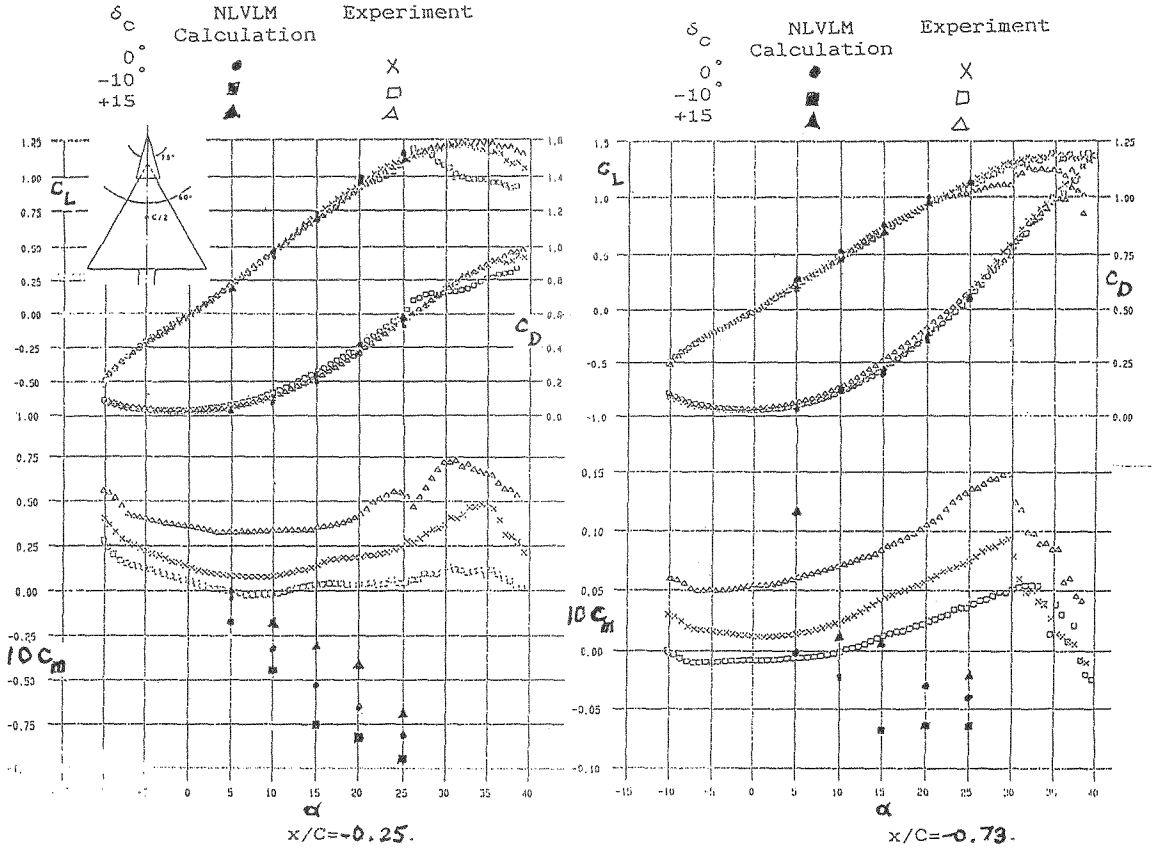

Fig. 11. The Variation of the Aerodynamic Coefficients as a function of α for the Technion Narrow Canard Model at δ_c= -10°, 0°, +15°

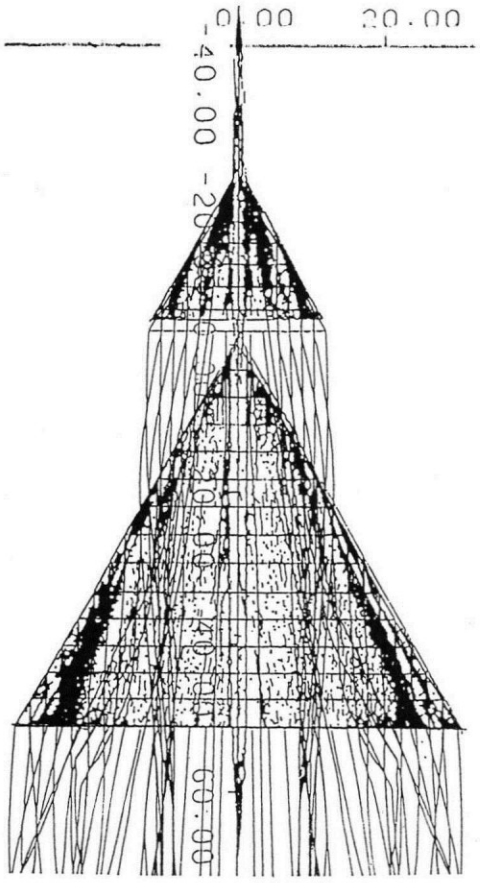

Fig. 12a. The Oil Flow Visualization on Model A at $\alpha = 8.8^{\circ}$ and the Calculated Vortex Trajectories by the NLVLM

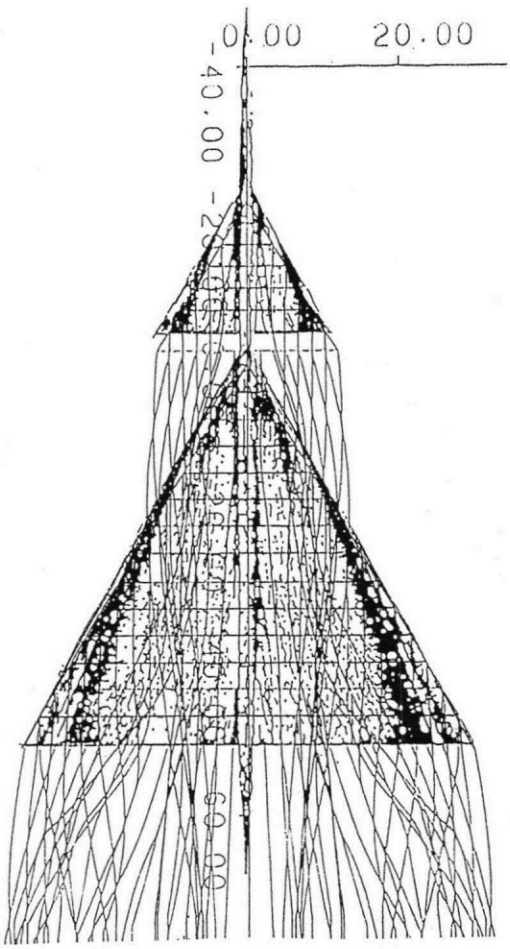

Fig. 12b. The Oil Flow Visualization on Model A at $\alpha = 14.7^{\circ}$ and the Calculated Vortex Trajectories by the NLVLM

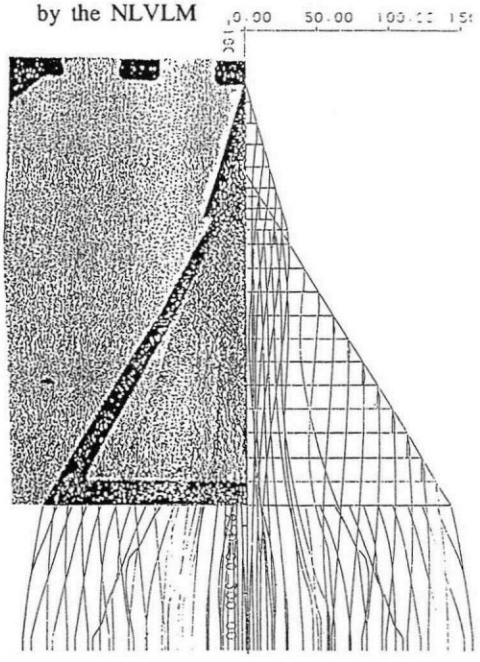

Fig. 13a. Schlieren Photograph Visualization on the Narrow Canard Model at $\alpha = 17^{\circ}$ and the Calculated Vortex Trajectories by the NLVLM - Top View

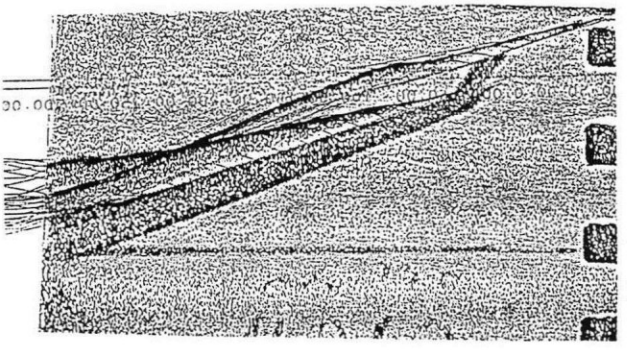

Fig. 13b. Schlieren Photograph Visualization on the Narrow Canard Model at $\alpha = 17^{\circ}$ and the Calculated Vortex Trajectories by the NLVLM - Side View

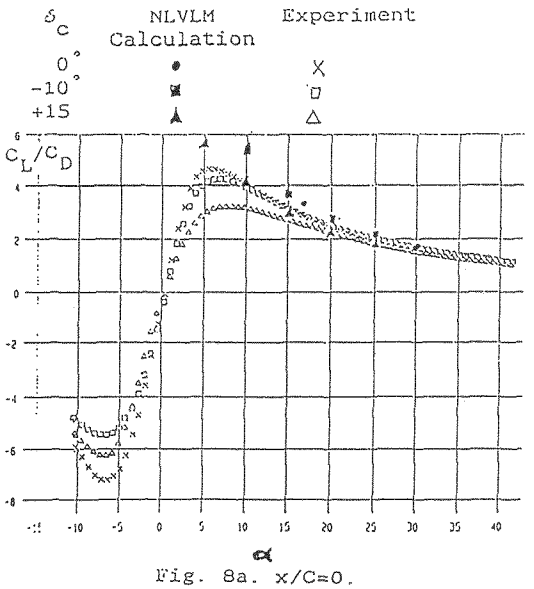

Fig. 8a. x/C=0.

Fig. 14. The Lift/Drag Ratio Variation as a function of α for the Wide Canard Model

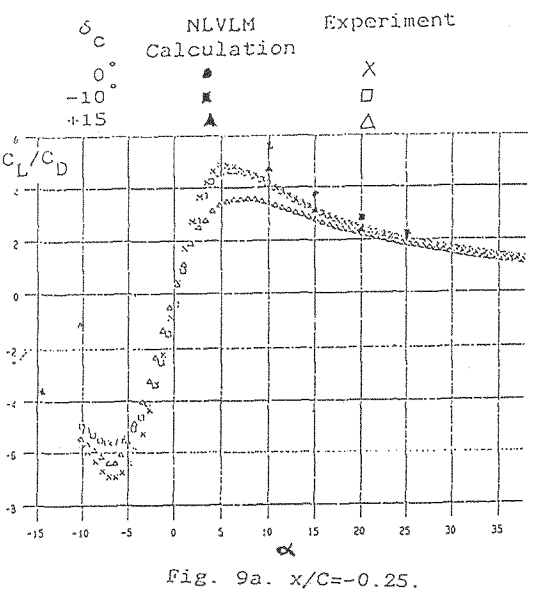

Fig. 9a. x/C=-0.25.

Fig. 15. The Lift/Drag Ratio Variation as a function of α for the Narrow Canard Model

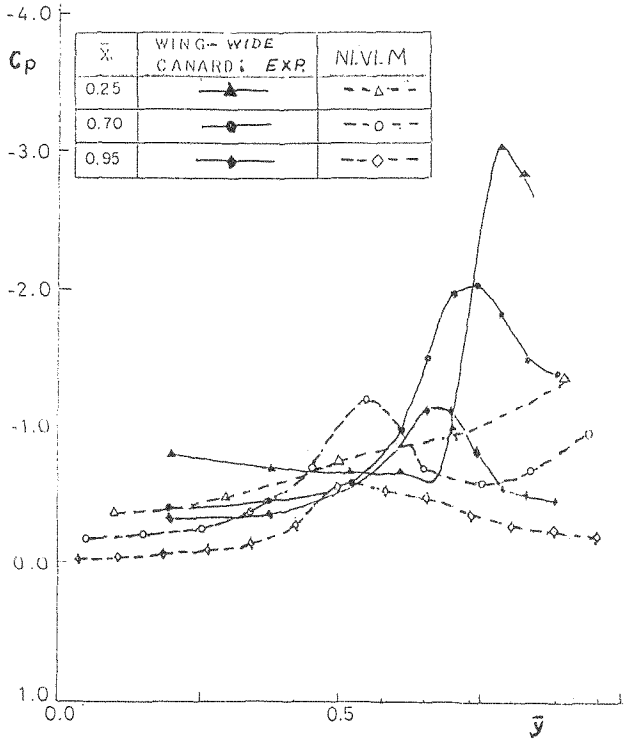

Fig. 16. The Pressure Distribution on the Wing of the Wide Canard Model at $\alpha = 18°$

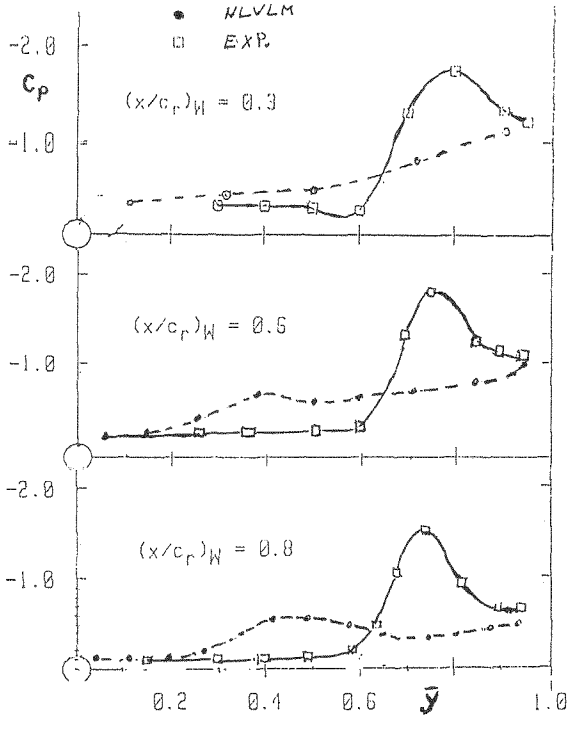

Fig. 17. The pressure Distribution on the Wing of the European Model B Configuration at $\alpha = 15°$